ChemistrySelect

Research Article
doi.org/10.1002/slct.202300874

Chemistry Europe
European Chemical Societies Publishing

www.chemistryselect.org

Noble Metal Nanoparticles Networks Stabilized by Rod-Like Organometallic Bifunctional Thiols

Sara Cerra,*[a] Laura Carlini,[b] Tommaso A. Salamone,[a] Farid Hajareh Haghighi,[a] Martina Mercurio,[a] Beatrice Pennacchi,[a] Carla Sappino,[a] Chiara Battocchio,[b] Stefania Nottola,[c] Roberto Matassa,[c] and Ilaria Fratoddi*[a]

Rod-like organometallic dithiol containing square-planar Pt(II) centers, i.e., trans,trans-[(H₃COCS)Pt(PBu₃)₂(C≡C—C₆H₄—C₆H₄—C≡C)(PBu₃)₂Pt(SCOCH₃)] was used as bifunctional stabilizing agent for the synthesis of Pd-, Au-, and AgNPs (MNPs). All the MNPs showed diameters of about 4 nm, which can be controlled by carefully modulating the synthesis parameters. Covalent MNPs stabilization occurred through a single S bridge between Pt(II) and the noble metal nanocluster surfaces, leading to a network of regularly spaced NPs with the formation of dyads, as supported by SR-XPS data and by TEM imaging analysis. The chemical nature of NPs systems was also confirmed by EDS and NMR. Comparison between SR-XPS data of MNPs and self-assembled monolayers and multilayers of pristine rod-like dithiols deposited onto polycrystalline gold surfaces revealed an electronic interaction between Pt(II) centers and biphenyl moieties of adjacent ligands, stabilizing the organic structure of the network. The possibility to obtain networks of regularly spaced MNPs opens outstanding perspectives in optoelectronics.

Introduction

In the last decade, there has been a large increase in the type and variety of nanostructured materials made by engineered nanoparticles and their applicative perspectives are widely addressed in the literature.[1] Among the variety of nano-materials, noble metal nanoparticles (MNPs) represent a unique class of functional systems characterized by peculiar physical and chemical properties that are markedly different from those elicited by the corresponding bulk materials.[2,3] A great contribution to the ability to modulate nanomaterial properties, as well as to stabilize the nanosystems, arises from their surface functionalization with appropriate organic molecules.[4–6] At the nanoscale, surface atoms exhibit incomplete valence since they are only bound to the internal atoms, thus keeping external sites available for interacting with appropriate ligands/function-alizing agents to prevent irreversible aggregation of colloidal nanoparticles.[7,8] Excellent stability towards aggregation can be achieved via thiols and thiol-derivatives capping agents, due to the strong affinity of thiol moieties for transition metal surfaces, giving rise to stable metal-sulfur (M—S) linkages.[9] Furthermore, ligands choice strongly influences size and shape of MNPs.[10] Chemically-capped gold and silver nanoparticles (AuNPs, AgNPs) show peculiar optical properties, e.g., localized surface plasmon resonance (LSPR) phenomenon, high chemical stability, catalytic and size-dependent electrochemical properties, antimicrobial and antibacterial behavior (especially AgNPs).[11–13] Although less investigated, thiol-functionalized palladium nanoparticles (PdNPs) show interesting properties that makes them suitable for applications in the field of sensing, electron transfer processes, photochemical and electronic devices.[14,15] As reported in literature, interparticle electromagnetic coupling effect, i.e., a cooperative effect of the surface plasmon resonances, arises for interparticle distances smaller than five times the cluster radius.[16] As a result of this phenomenon, a red-shift and broadening of Au- and AgNPs SPR band in the visible region occurs.[17,18] In this regard, the generation of ordered structures of metal NPs at large length scale is very challenging due to the demanding requirements for assembly precision. In the case of colloidal nanoparticles fine tuning of spatial resolution between NPs (particle size 3–20 nm, gap size ca. 5 nm)[19] can be achieved by self-assembly processes, i.e., the spontaneous process by which discrete building blocks

[a] Dr. S. Cerra, T. A. Salamone, F. Hajareh Haghighi, M. Mercurio, B. Pennacchi, Dr. C. Sappino, Prof. I. Fratoddi
Department of Chemistry
Sapienza University of Rome
P.le Aldo Moro 5, 00185 Rome, Italy
()
()
E-mail: sara.cerra@uniroma1.it
ilaria.fratoddi@uniroma1.it
Homepage: https://www.chem.uniroma1.it/en/department/people/sara-cerra
https://www.chem.uniroma1.it/en/department/people/ilaria-fratoddi

[b] Dr. L. Carlini, Prof. C. Battocchio
Department of Sciences
Roma Tre University
Via della Vasca Navale 79, 00146 Rome, Italy

[c] Dr. S. Nottola, Dr. R. Matassa
Department of Anatomical, Histological, Forensic and Orthopaedic Sciences, Section of Human Anatomy
Sapienza University of Rome
Via A. Borelli 50, 00161 Rome, Italy

ChemistrySelect

Research Article
doi.org/10.1002/slct.202300874

Chemistry Europe
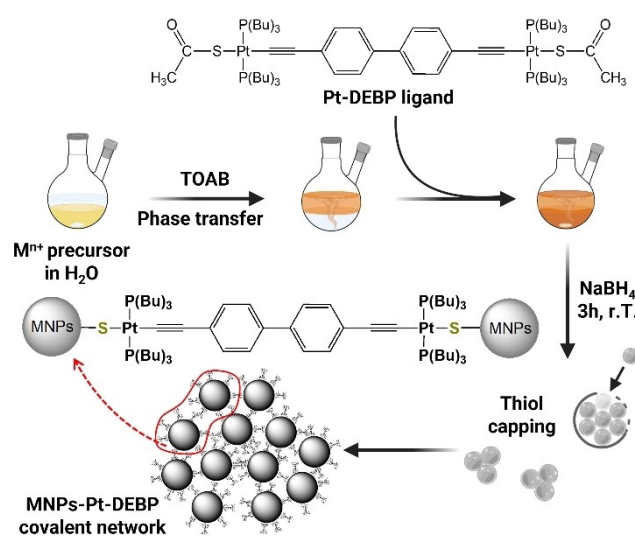European Chemical
Societies Publishing

organize themselves into ordered macroscopic structures that meet the requirements of efficiency, robustness, and reproducibility for practical applications.[20] To do so, nanoparticles can be functionalized to provide the chemical specificity and high precision interparticle gap control. As an example, DNA-functionalized NPs have emerged as a promising approach, since DNA length can be tuned according to the desired interparticle distances (number of bases).[21] Other interesting possibilities based on chemical surface functionalization include modification of soft organic shells (*e.g.*, alkanethiolates[22]) or photo-switchable molecules[23] to tune molecular interactions and create ordered assemblies of NPs. Alternatively, dewetting and Langmuir-Blodgett techniques can be used to obtain 2D ordered particle arrays on solid surfaces taking advantage of relatively weak attractive forces between NPs.[24,25] Particularly attracting is the covalent functionalization of MNPs surface with rigid bifunctional thiols that allow to synthesize networks of regularly spaced metal nanoparticles with finely tuned interparticle distances.[26,27] Herein, the one-pot synthesis of palladium nanoparticles (PdNPs) stabilized with the organometallic bifunctional thiol *trans,trans*-[dithioacetyldibis(tributylphosphine)diplatinum(II)-4,4'-diethynylbiphenyl] (hereafter reported as Pt-DEBP(SCOCH$_3$)$_2$) is reported. The aim is to assess the formation of a trinuclear covalent Pd-S-Pt bond between the bifunctional organometallic thiolate complex and PdNPs surface, as already studied with analogous Au and Ag-based nanosystems.[26,27] The size, shape and crystalline structure of these thiol functionalized palladium nanoparticles were determined by transmission electron microscopy (TEM), energy dispersive X-ray spectroscopy (EDS), ^{1}H and ^{31}P nuclear magnetic resonance (NMR), and high-resolution synchrotron radiation induced X-ray photoelectron spectroscopy (SR-XPS). The latter allowed to probe the intermolecular interaction occurring between adjacent rod-like dithiols, involving Pt(II) centers and biphenyl rings considerably stabilizing the organic moieties arrangement. In order to provide useful models to understand the complex data achieved on the as-synthesized PdNPs, self-assembled monolayers (SAM) and multilayers (MUL) of Pt-DEBP(SCOCH$_3$)$_2$ on gold surfaces were also prepared and investigated. Platinum(II) ethynylated complexes are excellent candidates for optoelectronics and sensing applications due to their well-assessed electronic properties that arise from inter- and intrachain charge transport mechanisms.[28]

Results and Discussion

Synthesis of NPs. PdNPs stabilized by the organometallic bifunctional thiol *trans,trans*-[dithiodibis(tributylphosphine)-diplatinum(II)-4,4'-diethynylbiphenyl] (Pt-DEBP(SCOCH$_3$)$_2$) (metal precursor/sulfur 2:1 molar ratio) were prepared by a modified two-phase wet chemical reduction method, as already reported for the synthesis of Au- and AgNPs.[26,27] During the synthesis, the organometallic thioester is subjected to an *in situ* deacetylation due to the presence of acidic conditions, in analogy to organic[29] and organometallic thioesters; this reaction promotes the formation of the S-metal bond.[30] The

final MNPs-Pt-DEBP were obtained following the one-pot procedure depicted in Scheme 1. Spectroscopic characterization of pristine Pt-DEBP(SCOCH$_3$)$_2$ ligand and Au-, Ag-, and PdNPs-Pt-DEBP and are reported in Figure S1 and Figure S2, respectively. However, for nanometer-sized PdNPs, the absorption profile does not feature a well-defined absorption such as surface plasmon resonance (SPR) band of AuNPs-Pt-DEBP (SPR$_{AuNPs}$ 525 nm) and AgNPs-Pt-DEBP (SPR$_{AgNPs}$ 420 nm); whereas, for PdNPs within 1–10 nm size range, only the Mie scattering profile can be observed, thus confirming the nanoparticles formation.[31] Powerful complementary information about the chemical composition at the surface of NPs were from energy dispersive X-ray spectroscopy (EDS), ^{1}H and ^{31}P nuclear magnetic resonance (NMR). Micro-analysis with EDS (Figure S3) verified the presence of the metal nanoparticles core (Pd, Ag, and Au), together with peaks associated to platinum, phosphorus, and sulfur of Pt-DEBP ligand. NMR spectra of AuNPs-Pt-DEBP dispersed in CDCl$_3$ are reported as representative sample in Figure S4. In the ^{1}H-NMR spectrum, the four resonances in the alkyl-proton region (0.90–2 ppm) can be assigned to –CH$_2$ and –CH$_3$ protons of tributylphosphine linked to Pt(II) centers, whereas resonances associated to aromatic DEBP moiety in the ligand structure can be seen in the 7.00–7.60 ppm region. Additionally, corresponding resonance due to internal phosphines on Pt(II) was observed in the ^{31}P-NMR spectrum at 3.09 ppm, in agreement with a square planar Pt(II) center in *trans* configuration.[32]

Morphological characterization of NPs. The morphology and surface modification of Au-, Ag-, and PdNPs-Pt-DEBP were investigated by transmission electron microscopy (TEM). The morphology and morphometric characterization of well-separated nanoparticles forming an extensive network are reported in Figure 1 (PdNPs-Pt-DEBP) and Figure S5 (Au- and AgNPs-Pt-DEBP). Bright-field (BF) transmission electron microscopy shows a monolayer of separated dark NPs deposited by drop casting from their colloidal suspensions on a carbon amorphous film.

Scheme 1. General synthesis procedure for MNPs-Pt-DEBP (M=Au, Ag, Pd).

ChemistrySelect

Research Article
doi.org/10.1002/slct.202300874

Chemistry Europe
European Chemical
Societies Publishing

Appropriate imaging analyses have been exploited to perform accurate quantitative measurements of the size and spatial distribution of individual nanoparticles, paying attention to the statistical analysis. Since all the nanoparticles systems seem assembled into a bi-dimensional monolayer network with regular spatial distributions, quantitative morphometric measurements and a possible topological relationship among the NPs have been investigated. In the case of PdNPs-Pt-DEBP, by measuring the diameter of 1555 selected palladium nanoparticles in enlarged statistical imaging analyses revealed an overlapping of a bimodal size distributions. The higher-counts distribution is centered at 3.35 ± 0.48 nm with a polydispersity of about 15%, while the second bin distribution of low-counts value is centered at 3.52 ± 0.36 nm with a polydispersity of about 10%. It should be noticed that the bimodal size distribution exhibits the smallest difference, and the applied synthesis was able to limit the growth of the nanoparticles. In fact, the histogram of the nanoparticle diameter clearly exhibits a linear increase of the dimension from about 2 nm to 3.5 nm and later a rapid decrease in counts can be observed, locking the growth mechanisms. A magnified region of the white line square evidences well separated PdNPs in which red rods of same length have been drawn among neighbor dark nanoparticles only to show that the unnatural rods could be associated to the organometallic spacer (Pt-DEBP, Inset of Figure 1a).[33] To explore how the organometallic bridge may have involved in the organization of the palladium interparticle distance into a 2D self-assembled network, an image analysis technique has been used to quantify the distribution among surface-to-surface nearest neighbor distances of about 2.1 nm. In order to obtain more experimental information on the 2D-network, selected area electron diffraction (SAED) measurements were performed for identifying the atomic and structural compositions of the observed hybrid aggregate. The corresponding electron diffraction pattern (EDP) exhibits diffraction rings produced by a random orientation of the polycrystalline material (Figure 1b). By measuring the d-spacing of the diffraction rings, we were able to identify the typical Pd crystallites with a face centered-cubic (fcc) structure of a space group Fm3m (American Mineralogist Crystal Structure Database, amcsd 0014952), confirmed also by the intensive ring of $d_{111} = 0.224$ nm (grey dot arcs). Similar TEM morphology and morphometric characterization have been already performed for gold and silver nanoparticles samples showing a well-organized 2D-network.[26,27] Therefore, BF-TEM and SAED observations have been reported Figure S5. Herein, imaging analysis estimated AuNPs and AgNPs diameter of 3.95 ± 0.56 nm and of 3.54 ± 0.62 nm closer to previous investigations, and the estimated interparticle distances remain similar to the length of the organometallic spacer Pt-DEBP of about 2.1 nm (theoretical S-to-S distance for Pt-DEBP ligand 2.034 nm[28]). To further support these results, in a previously published paper Li Voti et al. applied the photoacoustic spectroscopy (PAS) technique (listening to both the absorption and scattering phenomena generated by nanoparticles in liquid phase) for determining the mesoscale assembly of interconnected AgNPs-Pt-DEBP in chloroform. The results of PAS measurements showed that the

nanoparticles self-assembly detected at solid state by TEM is presents also on NPs floating in suspension.[34] To identify the atomic and structural compositions of the samples, SAED investigations have been probed. The corresponding EDPs of the AuNPs and AgNPs display several diffraction rings with different planes assigned to the typical Au and Ag crystallites both with a face centered-cubic (fcc) structure of a space group
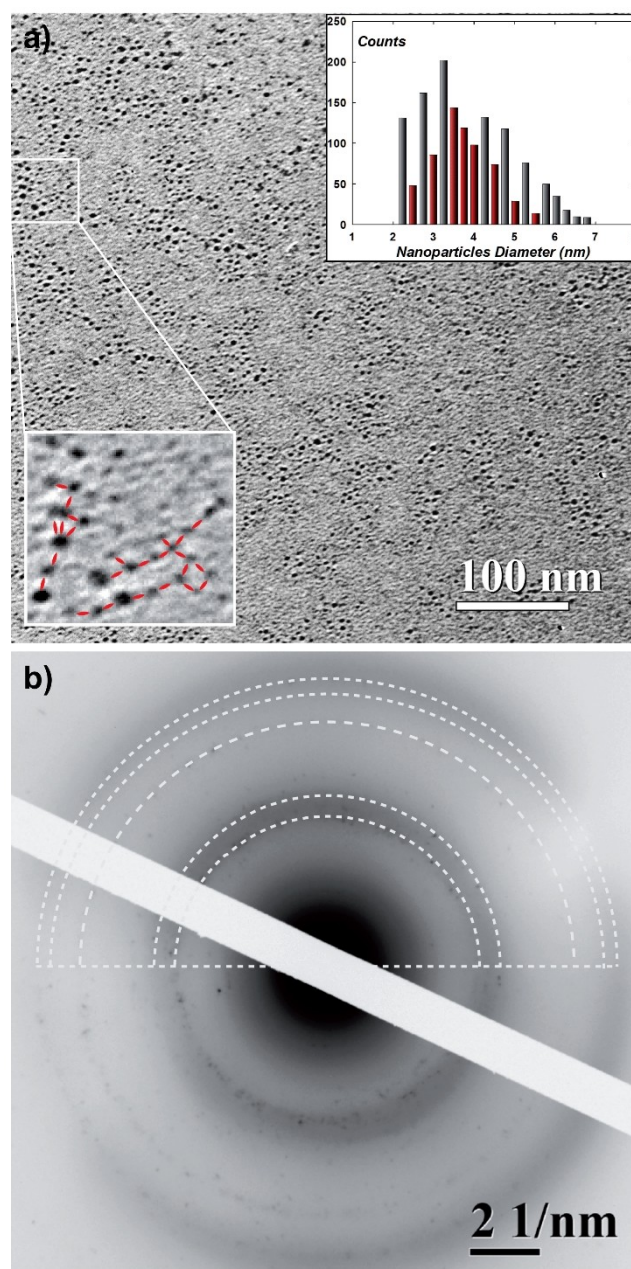

Figure 1. Morphological study of palladium nanoparticles self-assembled in a monolayer network by Pt-DEBP bifunctional organometallic thiols. (a) BF-TEM image of the inorganic-organic 2D-network of Pd-Pt-DEBP nanoparticles. Inset: magnified region (white square) showing similar distances among nanoparticles evidenced by red rods (bottom-left) and histogram plot shows the frequency distribution of the nanoparticle dimension (top-right) (b) EDP taken from Figure 1a showing distinct diffraction rings corresponding to the crystalline phases of Pd nanocrystal (grey dot line arcs).

ChemistrySelect

Research Article
doi.org/10.1002/slct.202300874

Chemistry
Europe
European Chemical
Societies Publishing

Fm3m, confirmed also by the intensive ring of $d_{111} = 0.236$ nm. These morphometric investigation of the noble metal NPs regarding the dimensions and their similar interparticle distances let us see the strong influence of the organometallic spacer that links covalently the surface of the NPs forming a

Figure 2. SR-XPS at a) Au4f$_{7/2,5/2}$ core level for AuNPs-Pt-DEBP, b) Ag3d$_{5/2,3/2}$ for AgNPs-Pt-DEBP and c) Pd3d$_{5/2,3/2}$ of PdNPs-Pt-DEBP.

self-assembled monolayer, independently from the noble metal species used through the wet-chemistry approach.

SR-Induced X-Ray Photoelectron Spectroscopy Investigation. With the aim to probe the chemical and electronic interaction at the interface between noble metal NPs and rod-like Pt-DEBP(SCOCH$_3$)$_2$ ligand, high resolution SR-XPS experiments were performed. Measurements were carried out at P2p, S2p, Pt4f, and Au4f or Pd3d or Ag3d core levels for all the considered samples (for complete BE, FWHM, atomic ratio values and assignments, see Table S1). Data collected on SAM and multilayer of the same molecules anchored on polycrystalline gold substrates (Au/Si(111) wafers) were also analyzed for comparison; in particular, the S2p signal analysis performed on SAM and multilayer samples was used as reference for the interpretation of the sulfur spectra collected on the stabilized NPs. For all the NPs samples, P2p$_{3/2}$ BE values were found at about 130 eV (Figure S6), whereas for Pt4f$_{7/2}$ at ca. 72.6 eV (Figure S7), as expected for binuclear compounds of Pt-DEBP-like Pt(II) dimers, evidencing that the organometallic molecules are all surface associated and that Pt-S bond cleavage and/or phosphines oxidation and degradation is not occurring, thus allowing to assess the ligands molecular structure stability after the synthesis procedure. Furthermore, SR-XPS measurements allowed to assess the anchoring of the organometallic thiols onto gold substrates as well as to gold, silver, and palladium nanoparticles surfaces. To characterize the chemical structure of the ligands on monolayers and multilayers, the metal and sulfur core level spectra were collected. For SAM, a single pair of spin-orbit components is detected in the Au4f signal with the main Au4f$_{7/2}$ component at 83.89 eV BE related to metallic gold atoms, as expected for a polycrystalline gold substrate covered by a very thin molecular substrate (monolayer).[26] In the multilayer sample, Au4f signal intensity is very low, due to the attenuation of the thick overlayer. Concerning the stabilized NPs, metal core-level signals (i.e., Pd3d, Au4f and Ag3d) were collected and analyzed (Figure 2). By a curve-fitting analysis, two spin-orbit pairs can be observed (in all cases) and associated to metal atoms involved in different chemical environments. Characteristically, the signal at lower BE values is attributed to metallic atoms in NPs bulk; on the other hand, the spectral component that occurs at a higher BE value is associated with metal sites coordinating the electron acceptor thiol ligands.[26] More in detail, in Au4f spectrum of AuNPs (Figure 2a) a main spin-orbit pair is found at BE values expected for the metallic gold signal (Au4f$_{7/2}$ BE = 83.87 eV), and a less intense couple of components at higher BE (Au4f$_{7/2}$ BE = 84.47 eV) coherently with positively charged Au atoms belonging to the NP surface and chemically interacting with sulfur (about 46% in the gold atomic percent); for the Ag3d SR-XPS spectrum of AgNPs (Figure 2b) two doublets can be observed: a main spin-orbit pair at 367.99 eV, as expected for metallic silver related to the core NPs atoms, and a second component at about 368.59 eV, associated to the surface metallic atoms involved in Ag—S—R bridges[27] and corresponding to a 44% in the atomic percent. Likewise, to probe the electronic interaction at PdNP/thiol interface, the Pd3d core level was measured (Figure 2c). The peak fitting procedure allows to
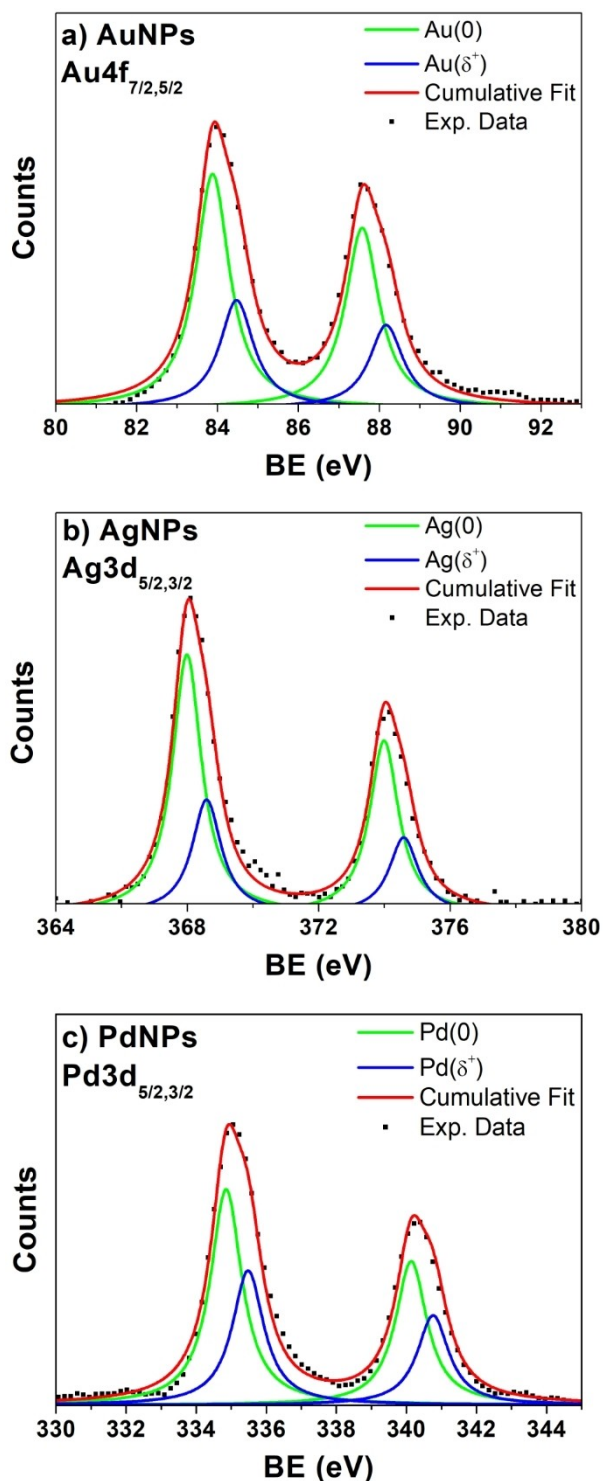
identify two pairs of spin-orbit doublets: the spin-orbit pair at lower BEs, $Pd3d_{5/2}$ BE = 334.85 eV, is due to the metallic palladium signal. The signal at higher BE (335.48 eV) is associated with palladium atoms that are partially positively charged because of the chemical bond with the thiol. The surface palladium atoms involved in the Pd-S bond correspond to a 62% in the atomic percent.

S2p spectra collected on SAM and multilayer provided useful references for the interpretation of NPs data, as reported in the following. As shown in Figure 3a, the sulfur signal collected on SAM shows two doublets ($S2p_{3/2}$ BE = 162.3 eV and $S2p_{3/2}$ BE = 163.3 eV), whereas for the multilayer sample (Figure 3b) only a single spin-orbit pair is detected, with the 3/2 component at about 163.3 eV in BE. According to the literature, the spin-orbit doublet at lower binding energy is due to organometallic thiols chemically linked to metals through a covalent S-metal bond, while the signal at higher BE values is associated with sulfur atoms of free thiol terminal groups.[35] It is noteworthy that the atomic ratio between the two components is 1:1 for SAM, suggesting the formation of a monolayer in which each molecule is anchored on the gold surface while preserving a free terminal group (inset in
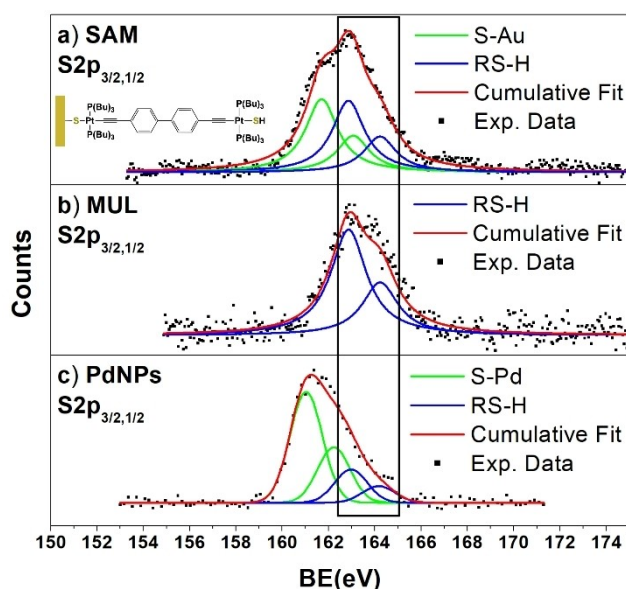
Figure 3a). Conversely, S2p spectra of AuNPs, AgNPs and PdNPs showed a single signal at low BE values, similarly to the low BE signal observed in SAM (*i.e.*, around 160–162 eV in BE) and attributed to organometallic thiols chemically bonded to metals through a S-metal bond,[24] suggesting that all thiol groups of MNPs are involved in sulfur-metal chemical bonds (S2p spectrum collected on PdNPs is reported as an example in Figure 3c, all the S2p spectra are reported in Figure S8). This finding supports the hypothesis of the formation of a NPs network organized in a "thiol bridges" configuration, coherently with TEM images. According to SAM and MUL spectra interpretation, in the PdNPs S2p spectrum (Figure 3c) two spin-orbit pairs can be found: at lower BEs the spin-orbit component is due to organometallic thiol chemically interacting with NPs surface through Pd-S covalent bond (77%), whereas signals at higher BE (162.97 eV) can be associated with sulfur atoms of free thiol end-groups (ca. 23%). The latter are due to a fraction of terminal sulfide groups not interacting with the NPs surface or physisorbed thiols.[36]

Pt4f SR-XPS spectra gave interesting information about the interaction between adjacent ligand molecules, as reported for similar systems.[26,27] Molecular self-assembling is commonly observed in films of polymeric conjugated systems containing transition metal centers σ- or π-bonded to organic main chain. For the here discussed samples, except for the SAM, all Pt4f spectra showed a second component at higher BE values (ca. 73–74 eV) respect to the previously discussed signal related to square-planar Pt(II). This secondary feature observed in Pt4f spectra can be attributed to the Pt atoms electronically interacting with the ethynyl-biphenyl groups of adjacent molecules, as expected for rod-like polyynes, giving rise to intra and inter-molecular charge transfer between metal and ligand. BE, FWHM, atomic ratio values and assignments of Pt4f collected on all the here presented samples are reported in the following Table 1.

As a matter of fact, a variety of d-transition metal complexes involving metal ions like Ru(II), Re(I), Pt(II) and Ir(III) show interesting optical properties related to inter- and intra-molecular charge transfer (CT). Among these metal complexes, square-planar Pt(II) complexes are quite interesting, since they show metal-to-ligand CT (MLCT), ligand-centered (LC), and/or metal-metal-to-ligand CT (MMLCT) optical emission, depending on ligand structure, temperature, medium and concentration.[37,38] It can be noticed a switching between metal-to-ligand charge transfer, intra-ligand charge transfer (ILCT), ligand-to-ligand charge transfer (LLCT), or intra-ligand

Figure 3. SR-XPS at $S2p_{3/2,1/2}$ core level of a) self-assembled monolayer (SAM), b) self-assembled multilayer (MUL) and c) PdNPs-Pt-DEBP. The component associated to the free thiol terminal group is highlighted.

Table 1. SR-XPS $Pt4f_{7/2}$ collected on SAM and MUL of Pt polyynes Pt-DEBP and on NPs stabilized by Pt-DEBP (BE, FWHM, atomic ratios and assignments).

Sample	BE	FWHM	I ratio[a]	Assignment
SAM	72.83	1.45	1	Pt-DEBP-like
MUL	72.59 73.44	1.74 1.74	85.05% 14.95%	Pt-DEBP-like Pt(δ^+)
AuNPs	72.61 73.59	1.68 1.68	84.60% 15.40%	Pt-DEBP-like Pt(δ^+)
AgNPs	72.63 73.34	1.64 1.64	82.13% 17.87%	Pt-DEBP-like Pt(δ^+)
PdNPs	72.80 74.04	1.82 1.82	77.69% 22.31%	Pt-DEBP-like Pt(δ^+)

[a] I ratio = I_{peak}/I_{tot} signal for the selected element.

ChemistrySelect

Research Article
doi.org/10.1002/slct.202300874

Chemistry Europe
European Chemical
Societies Publishing

(IL) transitions in platinum(II) complexes. These excited states might be interchanged by a change of solvent or pH, or by the introduction of metal ions, thereby yielding a variety of interesting photophysical properties.[39] Therefore the presence of a second doublet in the Pt4f of multilayer and NPs samples (Figure 4) seems to be due 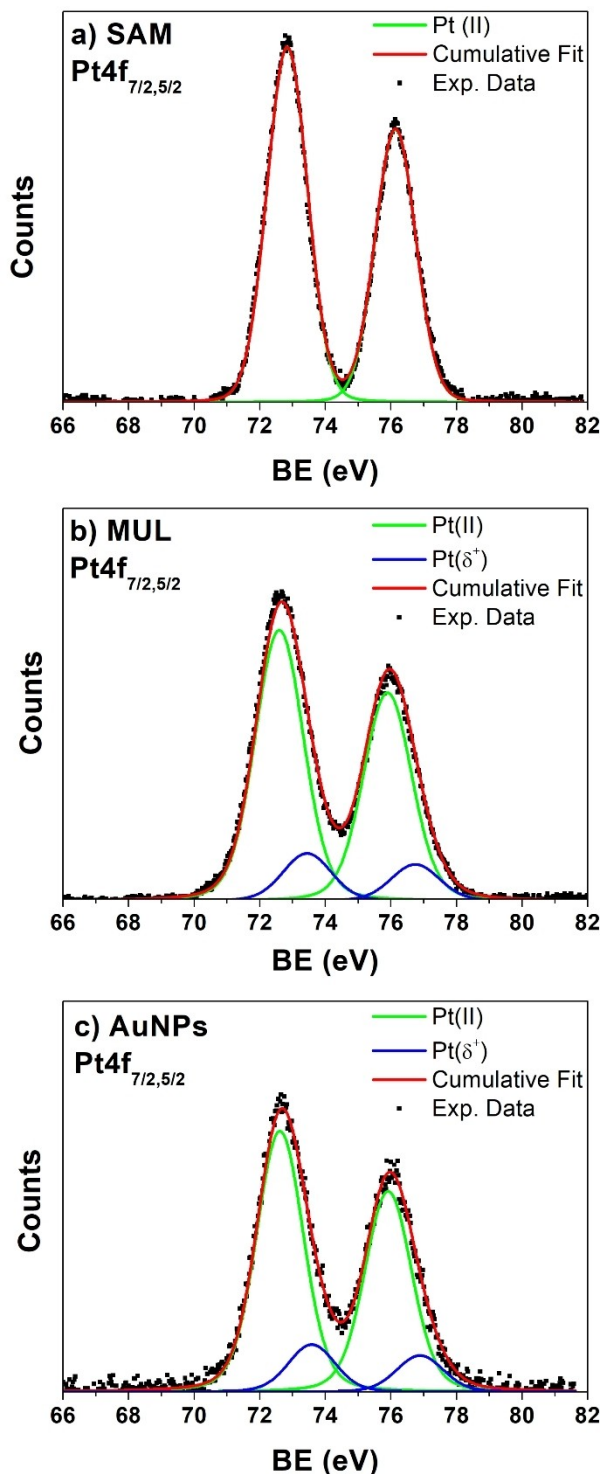to inter-chain interactions arising between metal centers and adjacent acetylene moieties and aromatic rings. This behavior in the self-assembling organization of dinuclear Pt(II)-based complexes and organometallic polyynes was already observed and reported in previous works.[40] Conversely, the Pt4f signal of SAM shows a single spin-orbit pair, confirming the formation of a monolayer without inter-chain interactions, [19] probably due to the larger interchain distances and/or to a different molecular packing that does not allow Pt-phenyl ring communication. Generally speaking, Pt4f and S2p spectra collected on SAM suggest the presence of a molecular orientation, as already observed in thin films of Pt-DEBP and Pd-DEBP deposited onto Au/Si(111) substrates and investigated by angular dependent NEXAFS spectroscopy;[41] this aspect will be subject to a future investigation.

Conclusion

The synthesis and characterization of palladium nanoparticles (PdNPs) stabilized by a novel bifunctional thiolate organometallic complex containing Pt(II) centers (PdNPs-Pt-DEBP) is reported and compared with Au- and AgNPs-Pt-DEBP. A self-assembled monolayer (SAM) and a multilayer (MUL) of the organometallic complex deposited onto a "flat" gold surface were prepared and investigated as a reference. UV-Visible spectroscopy allowed to confirm the nanoparticles formation, whereas EDS and ^{1}H,^{31}P-NMR were used to assess the chemical composition and the presence of Pt-DEBP ligand on the surface of NPs. The morphology of the nanoparticles was characterized by TEM analyses highlighting NPs with an average diameter of 3.35 ± 0.48 nm (PdNPs, as the higher-counts distribution), 3.95 ± 0.56 nm (AuNPs), and 3.54 ± 0.62 nm (AgNPs). The linkage between the PdNPs has an estimated interparticle distance of about 2.1 nm, in agreement with Pt-DEBP length. SR-XPS measurements allowed to assess the covalent attachment of the sulfur atoms as thiolates to the surface of metals. S2p spectra of PdNPs showed a single signal, suggesting that the organometallic dithiol can graft vicinal nanoparticles with both terminal groups in dyads, supporting TEM observations. The new hybrids show a direct link between Pt(II) and metal nanoparticles through a single S bridge, confirming the hypothesized achievement of 2D or 3D networks. Furthermore, the comparison between SR-XPS data collected on MNPs, SAM and MUL of the rod-like dithiols deposited onto a polycrystalline gold surfaces lead to ascertain that an electronic interaction occurs between the Pt(II) centers and the biphenyl moieties of adjacent ligands, stabilizing the organic part of the network. This behavior was observed for all noble-metal NPs, *i.e.*, AuNPs, AgNPs and PdNPs. In conclusion, the here demonstrated ability to obtain networks of regularly spaced noble metal nanoparticles (successfully tested on three different noble metals) opens outstanding perspectives in the field of optoelectronics.

Figure 4. SR-XPS at Pt4f$_{7/2,5/2}$ core level of a) self-assembled monolayer (SAM), b) self-assembled multilayer (MUL) and c) AuNPs-Pt-DEBP.

ChemistrySelect

Research Article
doi.org/10.1002/slct.202300874

Chemistry Europe
European Chemical
Societies Publishing

Experimental Section

Synthesis of the organometallic ligand. Bifunctional thiol *trans,-trans*-[dithioacetyldibis(tributylphosphine)diplatinum(II)-4,4'-diethynylbiphenyl] (Pt-DEBP) was prepared according to a previously published procedure and schematically reported in Figure S9.[26,27] The reaction is carried out in two steps: (i) the synthetic square-planar complex *cis*-Pt(PBu$_3$)$_2$Cl$_2$ (**1**) undergo to a dehydroalogenation reaction in the presence of 4,4'-diethynylbiphenyl (H–C≡C–C$_6$H$_4$–C$_6$H$_4$–C≡C–H, DEBP) to obtain the *trans,trans*-[ClPt-(PBu$_3$)$_2$-C≡C–C$_6$H$_4$–C$_6$H$_4$–C≡C–Pt(PBu$_3$)$_2$Cl] (**2**) complex; (ii) ligand exchange reaction of (**2**) in presence of potassium thioacetate led to the final Pt-DEBP(SCOCH$_3$)$_2$ (**3**) ligand.

Synthesis of metal nanoparticles. The gold, silver and palladium nanoparticles were prepared following a two-phase Schiffrin-Brust synthesis procedure. The molar ratio between the metal precursor and the Pt-DEBP(SCOCH$_3$)$_2$ ligand was 4/1. The PdNPs synthesis is presented as a typical procedure: an aqueous solution of K$_2$PdCl$_4$ (67.9 mg, 0.206 mmol) in deionized water (5 mL), was mixed with a solution of tetraoctylammonium bromide (TOAB) (134.8 mg, 0.251 mmol) in toluene (10 mL). The mixture was vigorously stirred until all the tetrachloropalladate was transferred into the organic phase and a solution of Pt-DEBP(SCOCH$_3$)$_2$ (80.2 mg, 0.052 mmol) in toluene (5 mL) was then added. The mixture was kept under Ar flux for 15 minutes and an aqueous solution of NaBH$_4$ (77.8 mg, 2.06 mmol) in deionized water (5 mL) was added under vigorous stirring. The reaction mixture was stirred for 3 h at room temperature. Then, the organic phase was separated, washed with water (7×10 mL) and further purified by repetitive centrifugation steps (10×10 mL ethanol) at 13,400 rpm, 15 min. The solid precipitate was collected and dried *in vacuo*. Yield: PdNPs = 12% (calculated as PdNPs/K$_2$PdCl$_4$ weight ratio).

Preparation of SAMs and multilayers of rod-like Pt(II) dithiol on polycrystalline gold surface. In order to prepare the self-assembled monolayer (SAM), the terminal thiol compound *trans,trans*-[(HS)-Pt(PBu$_3$)$_2$-C≡C–C$_6$H$_4$–C$_6$H$_4$–C≡C–Pt(PBu$_3$)$_2$(SH)] was obtained *in situ* by a deacetylation procedure carried out on the thioacetate precursor and allowed to self-assemble on polycrystalline gold surfaces (Au/Si(111) wafers surfaces). In a typical procedure, the Pt-DEBP(SCOCH$_3$)$_2$ ligand (30 mg, 0.019 mmol) was dissolved in 20 mL of THF and 260 μL of NH$_4$OH (30%) was added. The Pt-DEBP-(SCOCH$_3$)$_2$ solution was stirred at 30 °C for 2 h and filtered on celite. Gold-coated silica wafers were prepared by growing Au film 4000 Å thick onto Si(111) substrates and cut into slices (ca. 1 cm²), washed with several organic solvents (acetone, ethanol, chloroform), and blown dry with nitrogen. Freshly prepared gold substrates were dipped into the Pt-DEBP(SH)$_2$ solution for 4 h to achieve the anchoring of thiol on Au surface. The obtained multilayer was rinsed (ethanol, THF and acetone) to achieve the formation of a film in the monolayer thickness regime (SAM). The same procedure, without the final washing step, was applied to obtain Multilayer (MUL) sample. **Characterization techniques.** UV-vis spectra were carried out in CH$_2$Cl$_2$ solution by using 1 cm quartz cells with a Varian Cary 100 Scan UV-vis spectrophotometer in the 200–800 nm wavelength range. Resolution 1 nm. FTIR spectra have been recorded as films deposited by casting from CH$_2$Cl$_2$ solutions using KRS-5 (TlBr-TlI) cells, with a Bruker Vertex 70 spectrophotometer in the 4000–400 cm^{-1} wavenumber region (FTIR, resolution 4 cm^{-1}) and 500–200 cm^{-1} (FarIR, resolution 2 cm^{-1}). FarIR measurements were carried out by fluxing dry N$_2$ (100 L/h).

Energy dispersive X-ray (EDX) spectroscopy analyses were carried on an Auriga-Zeiss electron microscope. The sonicated samples were drop coated on aluminum or silicon stubs and air dried.

NMR spectra were recorded at 298 K on a Bruker Avance III instrument operating at the proton frequency of 400 MHz with the chemical shifts expressed in ppm. The chemical shifts were expressed from CDCl$_3$ (s, 7.24 ppm). ^{1}H-NMR spectra were acquired with 32 transients, a spectral width of 6009.15 Hz and 64 K data points. The recycle delay was set to 6.55 s in order to achieve complete resonance relaxation between successive scansions. ^{31}P-NMR spectra were acquired with 32 transients, 64 K data points and recycle delay of 2.00 s.

TEM images and Electron Diffraction Patterns (EDP) were captured using a ZEISS EM10 TEM operating at 80 keV.

Synchrotron radiation induced X-ray Photoelectron Spectroscopy experiments were performed at ELETTRA storage ring using the BACH (Beamline for Advanced DiCHroism) beamline and relative experimental station that is connected to an undulator front-end. Photoelectron spectroscopy was performed in the fixed analyser transmission mode with the pass energy set to 50 eV. Photons of 376 eV have been used for C1s, S2p, P2p, Pt4f and Au4f spectral regions; photon energy of 596 eV was chosen to acquire data at the Ag3d and Pd3d core-levels. Both monochromator entrance and exit slits were fixed at 30 μm. Calibration of the energy scale was made by referencing all the gold-containing spectra to the gold Fermi edge, and the Au 4f$_{7/2}$ signal was always found at 83.90 eV. For samples that did not contain gold, (AgNPs, PdNPs), the signal arising by the noble metal metallic atoms at NPs bulk was used, and a check was also made by with the aliphatic C1s component expected at 285.00 eV. The achieved resolving power was of 0.22 eV. Curve-fitting analysis of the P2p, Pt4f, S2p, Au4f, Pd3d and Ag3d spectra was performed using Voigt curves as fitting functions, after Shirley's background subtraction. S2p$_{3/2,1/2}$, Ag3d$_{5/2,3/2}$, Pd3d$_{5/2,3/2}$, Au4f$_{7/2,5/2}$ and Pt4f$_{7/2,5/2}$ doublets were fitted by using the same full width at half-maximum (FWHM) for each pair of components of the same core level, a spin-orbit splitting of, respectively, 1.2 eV, 6.0 eV, 5.3 eV, 3.7 eV and 3.3 eV and branching ratios S2p$_{3/2}$/S2p$_{1/2}$ = 2/1, Ag3d$_{5/2}$/Ag3d$_{3/2}$ = 3/2, Pd3d$_{5/2}$/Pd3d$_{3/2}$ = 3/2, Au4f$_{7/2}$/Au4f$_{5/2}$ = 4/3 and Pt4f$_{7/2}$/Pt4f$_{5/2}$ = 4/3. When several different species were individuated in a spectrum, the same FWHM value was used for all individual photoemission bands.

Supporting Information Summary

UV-Visible and FT-IR spectra of organometallic ligand. UV-Visible spectra of metal nanoparticles. EDS spectra of metal nanoparticles. ^{1}H-NMR, ^{31}P-NMR spectra of gold nanoparticles. TEM images of gold and silver nanoparticles. P2p, Pt4f, S2p core level XPS spectra of metal nanoparticles. Synthesis scheme of organometallic ligand. Full BE, FWHM and atomic ratio values and assignments of metal nanoparticles XPS analysis.

ChemistrySelect

Research Article
doi.org/10.1002/slct.202300874

Chemistry Europe
European Chemical
Societies Publishing

Conflict of Interest

The authors declare no conflict of interest.

Data Availability Statement

The data that support the findings of this study are available from the corresponding author upon reasonable request.

[1] S. S. Salem, E. N. Hammad, A. A. Mohamed, W. El-Dougdoug, *Biointerface Res. Appl. Chem.* **2023**, *13*, 41.

[2] D. Holec, P. Dumitraschkewitz, D. Vollath, F. Dieter Fischer, *Nanomaterials* **2020**, *10*, 484.

[3] T. Islam, R. Saenz-Arana, H. Wang, R. Bernal, J. C. Noveron, *New J. Chem.* **2018**, *42*, 6472–6478.

[4] N. Sun, S.-T. Zhang, F. Simon, A. M. Steiner, J. Schubert, Y. Du, Z. Qiao, A. Fery, F. Lissel, *Angew. Chem. Int. Ed.* **2021**, *60*, 3912–3917; *Angew. Chem.* **2021**, *133*, 3958–3963.

[5] S. Cerra, P. Pica, M. Congiu, M. H. Boratto, C. F. O. Graeff, I. Fratoddi, *J. Mater. Sci. Mater. Electron.* **2020**, *31*, 12083–12088.

[6] L. R. Pokhrel, B. Dubey, P. R. Scheuerman, *Environ. Sci. Technol.* **2013**, *47*, 12877–12885.

[7] R. L. Jaiswal, B. K. Pandey, *SN Appl. Sci.* **2021**, *3*, 466.

[8] N. K. Katiyar, K. Biswas, C. S. Tiwary, L. D. Machado, R. K. Gupta, *Langmuir* **2019**, *35*, 2668–2673.

[9] H. Häkkinen, *Nat. Chem.* **2012**, *4*, 443–455.

[10] S. Mozaffari, W. Li, M. Dixit, S. Seifert, B. Lee, L. Kovarik, G. Mpourmpakis, A. M. Karim, *Nanoscale Adv.* **2019**, *1*, 4052–4066.

[11] A. Szalai, Á. Sipos, E. Csapó, L. Tóth, M. Csete, I. Dékány, *Plasmonics* **2013**, *8*, 53–62.

[12] S. Manivannanm, R. Ramaraj, *Pure Appl. Chem.* **2011**, *83*, 2041–2053.

[13] A. Salleh, R. Naomi, N. D. Utami, A. W. Mohammad, E. Mahmoudi N. Mustafa, M. B. Fauzi, *Nanomaterials* **2020**, *10*, 1566.

[14] X. Tang, P.-A. Haddad, N. Mager, X. Geng, N. Reckinger, S. Hermans, M. Debliquy, J.-P. Raskin, *Sci. Rep.* **2019**, *9*, 3653.

[15] M. Vadai, D. K. Angell, F. Hayee, K. Sytwu, J. A. Dionne, *Nat. Commun.* **2018**, *9*, 4658.

[16] S. K. Ghosh, T. Pal, *Chem. Rev.* **2007**, *107*, 4797–4862.

[17] A. Mizuno, A. Ono, *Appl. Surf. Sci.* **2019**, *480*, 846–850.

[18] V. Sharma, D. Verma, G. S. Okram, *J. Phys. Condens. Matter* **2020**, *32*, 145302.

[19] S. Gwo, H.-Y. Chen, M.-H. Lin, L. Sun, X. Li, *Chem. Soc. Rev.* **2016**, *45*, 5672–5716.

[20] J. F. Galisteo-López, M. Ibisate, R. Sapienza, L. S. Froufe-Pérez, Á. Blanco, C. López, *Adv. Mater.* **2011**, *23*, 30–69.

[21] M. R. Jones, N. C. Seeman, C. A. Mirkin, *Science* **2015**, *347*, 1260901.

[22] I.-H. Kim, J. H. Kim, J.-Y. Choi, C. H. Shin, J.-H. Kim, G.-T. Bae, K. S. Shin, *Chem. Phys. Lett.* **2019**, *715*, 91–99.

[23] G. Sobczak, I. Misztalewska-Turkowicz, V. Sashuk, *J. Phys. Chem. C* **2021**, *125*, 5306–5314.

[24] X. Qi, J. Bi, *Opt. Commun.* **2019**, *453*, 124328.

[25] M. Tahghighi, D. Janner, J. Ignes-Mullol, *Nanomaterials* **2020**, *10*, 2264.

[26] I. Fratoddi, I. Venditti, C. Battocchio, G. Polzonetti, F. Bondino, M. Malvestuto, E. Piscopiello, L. Tapfer, M. V. Russo, *J. Phys. Chem. C* **2011**, *115*, 15198–15204.

[27] C. Battocchio, I. Fratoddi, L. Fontana, E. Bodo, F. Porcaro, C. Meneghini, I. Pis, S. Nappini, S. Mobilio, M. V. Russo, G. Polzonetti, *Phys. Chem. Chem. Phys.* **2014**, *16*, 11719.

[28] C. Battocchio, F. D'Acapito, I. Fratoddi, A. La Groia, G. Polzonetti, G. Roviello, M. V. Russo, *Chem. Phys.* **2006**, *328*, 1–3.

[29] S. Iimura, K. Manabe, S. Kobayashi, *Org. Lett.* **2003**, *5*, 101–103.

[30] S. Cerra, L. Fontana, E. Rossi, M. Bassetti, C. Battocchio, I. Venditti, L. Carlini, R. Matassa, G. Familiari, I. Fratoddi, *Inorg. Chim. Acta* **2021**, *516*, 120170.

[31] S. Chen, K. Huang, J. A. Stearns, *Chem. Mater.* **2000**, *12*, 540–547.

[32] F.-R. Dai, H.-M. Zhan, Q. Liu, Y.-Y. Fu, J.-H. Li, Q.-W. Wang, Z. Xie, L. Wang, F. Yan, W.-Y. Wong, *J. Chem. Eur. J.* **2011**, *18*, 1502–1511.

[33] R. Matassa, I. Fratoddi, M. Rossi, C. Battocchio, R. Caminiti, M. V. Russo, *J. Phys. Chem. C* **2012**, *116*, 15795–15800.

[34] R. Li Voti, G. Leahu, C. Sibilia, R. Matassa, G. Familiari, S. Cerra, T. A. Salamone, I. Fratoddi, *Nanoscale Adv.* **2021**, *3*, 4692–4701.

[35] D. Nilsson, S. Watcharinyanon, M. Eng, L. Li, E. Moons, L. S. O. Johansson, M. Zharnikov, A. Shaporenko, B. Albinsson, J. Mårtensson, *Langmuir* **2007**, *23*, 6170–6181.

[36] N. Kamatham, O. A. Ibraikulov, P. Durand, J. Wang, O. Boyron, B. Heinrich, T. Heiser, P. Lévêque, N. Leclerc, S. Méry, *Adv. Funct. Mater.* **2021**, *31*, 2007734.

[37] S. Roy, A. A. Lopez, J. E. Yarnell, F. N. Castellano, *Inorg. Chem.* **2022**, *61*, 121–130.

[38] M. Mauro, A. Aliprandi, D. Septiadi, S. Kehr, *Chem. Soc. Rev.* **2014**, *43*, 4144–4166.

[39] Y. Zhu, K. Luo, L. Zhao, H. Ni, Q. Li, *Dyes Pigm.* **2017**, *145*, 144–151.

[40] A. F. Suleymanova, Y. A. Yakovleva, O. S. Eltsov, A. O. Lantushenko, M. P. Evstigneev, B. Donnio, B. Heinrich, V. N. Kozhevnikov, *J. Organomet. Chem.* **2021**, *938*, 121750.

[41] C. Battocchio, I. Fratoddi, M. V. Russo, V. Carravetta, S. Monti, G. Iucci, F. Borgatti, G. Polzonetti, *Surf. Sci.* **2007**, *601*, 3943–3947.